

Propagation of toxic substances in the urban atmosphere: A complex network perspective

Original

Propagation of toxic substances in the urban atmosphere: A complex network perspective / Fellini, Sofia; Salizzoni, Pietro; Soulhac, Lionel; Ridolfi, Luca. - In: ATMOSPHERIC ENVIRONMENT. - ISSN 1352-2310. - ELETTRONICO. - 198:(2019), pp. 291-301. [10.1016/j.atmosenv.2018.10.062]

Availability:

This version is available at: 11583/2716997 since: 2018-11-11T12:35:31Z

Publisher:

Elsevier

Published

DOI:10.1016/j.atmosenv.2018.10.062

Terms of use:

This article is made available under terms and conditions as specified in the corresponding bibliographic description in the repository

Publisher copyright

Elsevier postprint/Author's Accepted Manuscript

© 2019. This manuscript version is made available under the CC-BY-NC-ND 4.0 license
<http://creativecommons.org/licenses/by-nc-nd/4.0/>. The final authenticated version is available online at:
<http://dx.doi.org/10.1016/j.atmosenv.2018.10.062>

(Article begins on next page)

Manuscript Number:

Title: Propagation of toxic substances in the urban atmosphere: a complex network perspective

Article Type: Research Paper

Keywords: Urban air pollution; Street network; Complex networks; Vulnerability; Accidental releases; Spreading on networks.

Corresponding Author: Miss Sofia Fellini, M.Eng.

Corresponding Author's Institution: POLITECNICO DI TORINO

First Author: Sofia Fellini, M.Eng.

Order of Authors: Sofia Fellini, M.Eng.; Pietro Salizzoni; Lionel Soulhac; Luca Ridolfi

Abstract: The accidental or malicious release of toxic substances in the urban atmosphere is a major environmental and safety problem, especially in large cities. Computational fluid dynamics codes and simplified modelling tools have been used in the last decades to model pollutant dispersion in urban areas. These studies have shown that propagation is strongly influenced by the layout of buildings and, therefore, by the street topology of the city. This work presents a novel approach to the study of toxic propagation within the urban canopy based on the theory of complex networks. Following recent studies on the development of urban dispersion models, the urban canopy is modelled as a network: the streets and the street intersections represent respectively the links and the nodes of the network. The direction and the weights of the links contain the geometric characteristics of the street canyons and their wind conditions. Within this approach, propagation is modelled as a spreading process on networks and a depth-first search algorithm is used to rapidly delimit the zone of influence of a source node. This zone is the set of streets that are contaminated from the source. As a case study, the proposed model is applied to the urban tissue of the city of Lyon. The algorithm simulates a toxic release in all the nodes of the network and identifies the number of people affected by each propagation process. In this way, vulnerability maps of the city are constructed. Moreover, various wind and concentration scenarios are easily implemented. These results evidence how the proposed method is effective for the rapid assessment of the most vulnerable points in a city, avoiding the use of long numerical simulations.



**POLITECNICO
DI TORINO**

Department of
Environment, Land and
Infrastructure Engineering

Torino, July 16, 2018

To:
Editorial Board of Atmospheric Environment

Subject: Manuscript Submission

Dear Editor,

we are enclosing herewith the manuscript entitled "Propagation of toxic substances in the urban atmosphere: a complex network perspective" for consideration of publication in Atmospheric Environment. With the present submission, we undertake the responsibility that the above-mentioned manuscript is original and has not been published nor is currently under consideration for publication elsewhere.

The research reported in this manuscript proposes an innovative approach for the study of pollutant dispersion within the urban canopy. This new approach is based on the promising theory of complex networks and allows us to model propagation from a source point as a spreading process on networks. In this way, the area of a city affected by a toxic release can be delimited with very low computational costs and vulnerability maps of urban areas can be rapidly constructed.

Our research is of interest for many disciplines, from urban meteorology to complex network science, and makes a significant step forward in the field of atmospheric fluid dynamics. Moreover, our methodology provides interesting tools for relevant current issues like urban pollution mitigation and terrorism prevention. We are thus confident that it is appropriate for publication in Atmospheric Environment.

All authors approved the manuscript and this submission. We know of no conflicts of interest associated with this publication. For any further clarification, do not hesitate to contact us.

We wish to thank you for your consideration and attention.

Best Regards,

Sofia Fellini
Pietro Salizzoni
Lionel Soulhac
Luca Ridolfi

1 Propagation of toxic substances in the urban 2 atmosphere: a complex network perspective

3 Sofia Fellini^{a,b,*}, Pietro Salizzoni^b, Lionel Soulhac^b, Luca Ridolfi^a

4 ^a*Department of Environmental, Land, and Infrastructure Engineering, Politecnico di*
5 *Torino, Corso Duca degli Abruzzi 24, 10129 Turin, Italy*

6 ^b*Laboratoire de Mécanique des Fluides et d'Acoustique, UMR CNRS 5509, Université de*
7 *Lyon, Ecole Centrale de Lyon, INSA Lyon, Université Claude Bernard Lyon I, 36, avenue*
8 *Guy de Collongue, 69134 Ecully, France*

9 Abstract

10 The accidental or malicious release of toxic substances in the urban atmo-
11 sphere is a major environmental and safety problem, especially in large cities.
12 Computational fluid dynamics codes and simplified modelling tools have been
13 used in the last decades to model pollutant dispersion in urban areas. These
14 studies have shown that propagation is strongly influenced by the layout of
15 buildings and, therefore, by the street topology of the city. This work presents
16 a novel approach to the study of toxic propagation within the urban canopy
17 based on the theory of complex networks. Following recent studies on the devel-
18 opment of urban dispersion models, the urban canopy is modelled as a network:
19 the streets and the street intersections represent respectively the links and the
20 nodes of the network. The direction and the weights of the links contain the ge-
21 ometric characteristics of the street canyons and their wind conditions. Within
22 this approach, propagation is modelled as a spreading process on networks and
23 a depth-first search algorithm is used to rapidly delimit the zone of influence of
24 a source node. This zone is the set of streets that are contaminated from the
25 source. As a case study, the proposed model is applied to the urban tissue of
26 the city of Lyon. The algorithm simulates a toxic release in all the nodes of
27 the network and identifies the number of people affected by each propagation
28 process. In this way, vulnerability maps of the city are constructed. Moreover,
29 various wind and concentration scenarios are easily implemented. These results

*Corresponding author
Preprint submitted to Journal of LATEX TeXnics (Sofia Fellini)

30 evidence how the proposed method is effective for the rapid assessment of the
31 most vulnerable points in a city, avoiding the use of long numerical simulations.
32 *Keywords:* Urban air pollution, Street network, Complex networks,
33 Vulnerability, Accidental releases, Spreading on networks

34 1. Introduction

35 Large cities are particularly vulnerable to air pollution as they exhibit both a
36 large number of potential sources and a high density of people exposed (Brunekreef
37 and Holgate, 2002; Heinrich and Wichmann, 2004). Urban air pollution is
38 mainly linked to human activities and in particular to vehicular traffic, heating of
39 buildings and industrial emissions (Mayer, 1999). Moreover, accidental releases
40 such those related to gas leaks, industrial plants or the transport of dangerous
41 goods are particularly critical in densely populated environments. Besides un-
42 intentional releases, the current political situation also raises the possibility of
43 terrorist attacks aimed at the dispersal of toxic or pathogenic substances in the
44 air (Tucker, 2000; McLeish, 2017).

45 For these reasons, local administrations are urged to adopt not only instru-
46 ments for air quality control but rather predictive tools for the management of
47 dangerous situations due to accidental and malicious releases. These actions are
48 in line with the current challenge of building resilient metropolises able to cope
49 with emergencies (Berke et al., 2009; Ahern, 2011).

50 Dispersion models are commonly used to predict urban pollution and to es-
51 timate concentration of toxic substances. Computational fluid dynamics (CFD)
52 simulations are the most suitable tool for modelling dispersion in a complex
53 geometry like the urban fabric, since they solve the velocity and concentration
54 field in the whole domain (Blocken, 2015). However, these models require a huge
55 computational cost and therefore long simulation times and high performance
56 computers. To reduce the computational cost, several modelling approaches
57 have been developed in the last decades (Di Sabatino et al., 2013). These in-
58 clude street network models (e.g., Carruthers et al., 2000; Soulhac et al., 2011)

59 based on a simplified description of the building geometry and modelling the
60 mass exchange within and above the urban canopy by parametrising few key
61 transfer processes. Their formulation rely on the basic idea that the urban
62 structure of the city, the orientation of the streets and their connectivity play a
63 major role in determining the intensity of these transfer processes.

64 Starting from these considerations, this work presents a novel approach for
65 the study of toxic pollutant dispersion within the urban canopy. The aim is
66 to evaluate rapidly and with negligible computational cost the vulnerability
67 of a dense city to the release of harmful airborne pollutants by means of the
68 modern techniques provided by the theory of complex network. According to
69 this perspective, propagation phenomena in the streets are represented as a
70 transport process on a network.

71 In complex network theory (e.g., Boccaletti et al., 2006; Newman, 2010),
72 complex systems are traced back to a set of entities (nodes) that interact with
73 each other. Interactions are represented as links between the nodes and may
74 have weights that describe the strength of these interactions. Complexity does
75 not lie in the elements that form the system, but rather in their topology and
76 within the pattern of their interconnections. In the last few years, the theory of
77 complex networks has gained a great attention in countless fields, from the social
78 sciences (e.g., Borgatti et al., 2009) to engineering (e.g., Carvalho et al., 2009;
79 Yazdani and Jeffrey, 2011; Giustolisi and Ridolfi, 2014). Recently, a network
80 approach has been adopted for the description of geophysical fluid motion and
81 associated transport phenomena. Gelbrecht et al. (2017) propose a complex
82 network representation of wind flows to study regional meteorology systems,
83 while Ser-Giacomi et al. (2015) represent mixing and dispersion processes in the
84 Mediterranean as a transportation network.

85 In this work we focus on the pollutant dispersion at the local urban scale.
86 The topology of the city is modelled as a network, within which the propagation
87 of the airborne toxic pollutant occurs. The streets and the street intersections
88 are respectively the links and the nodes of the network. The direction and the
89 weight of the links contain the fluid-dynamics properties of the flow within the

90 streets and the geometric characteristics of the bordering buildings. In this
91 way, the topology of the city and the wind conditions along the streets are all
92 represented in a single mathematical structure, that is a weighted and directed
93 complex network. Given an initial point, i.e. a pollutant source, the pathways
94 of propagation along the streets can be immediately predicted by this schematic
95 representation. In particular, as in epidemics applications (Newman, 2002), a
96 search algorithm on networks is adopted to delimit the zone of influence of a
97 source node, that we define as the part of the network affected by toxic propa-
98 gation. By applying this procedure to each node in the network, vulnerability
99 maps can be easily constructed and the urban areas with the highest spreading
100 potential are revealed at a glance. The method is fast and can be applied to
101 entire cities with a low computational cost.

102 The final aim is to provide a reliable and rapid method to (i) identify the
103 most vulnerable points in the city, i.e. the source points from which the toxic
104 spreading can affect the greatest number of people, and (ii) to understand the
105 effect of wind conditions on urban vulnerability. To this purpose, the method-
106 ological tools of network analysis are adopted and long numerical simulation of
107 dispersion processes are avoided.

108 The work is organized as follows. In Section 2, we describe the physical as-
109 sumptions adopted to model pollutant propagation in the urban canopy. Then,
110 the network perspective is introduced in Section 3. The basic steps to con-
111 struct the street network and its weight matrices are thus described and the
112 algorithm for spreading on networks is presented. Subsequently, the proposed
113 general method is applied to the city of Lyon (France). Vulnerability maps
114 for a district of Lyon are shown and analysed in Section 4. Finally, the main
115 conclusions obtained from the presented work are summarized.

116 **2. Physical assumptions about the propagation of a toxic substance** 117 **in the urban environment**

118 Transport and mixing processes in the urban environment are characterized
119 by complex fluid structures due to the interaction between the atmospheric
120 flow and the city. The presence of buildings and vegetation highly affects the
121 structure of the urban boundary layer, characterized by the generation of a
122 shear layer at the top of the canopy, wake diffusion behind buildings, and form
123 drag due to the pressure differences across the roughness elements (Roth, 2000).
124 Moreover, the flow field in the streets is altered by the convective fluxes due
125 to the differential solar irradiance on building walls and to the heat sources
126 related to human activities (Oke, 1982; Arnfield, 2003). The simulation of all
127 these dynamical effects on the flow field within the urban canopy is nowadays a
128 challenge for modellers that adopt sophisticated computational tools, typically
129 CFD codes (Tominaga and Stathopoulos, 2012). These require a huge amount of
130 input data and high computational costs, which limit their use when analysing
131 a large number of emission scenarios. In this latter case, alternative simulation
132 strategies should be adopted, based on a simplified description of the flow and
133 of the dispersion phenomena occurring within the urban fabric.

134 The physical assumptions for the propagation model presented in this work
135 are based on a street network approach (e.g., Namdeo and Colls, 1996; Soulhac
136 et al., 2011). The geometry of the urban canopy is simplified to a network of
137 streets (Fig. 1.a), and the streets are represented as urban canyons, i.e. cavities
138 of rectangular section with length l , height h and width w (Fig. 1.b). Following
139 the approach of Soulhac et al. (2011), the main transport phenomena for a
140 airborne pollutant in the urban canopy are (i) the convective mass transfer
141 along the street due to the mean wind along the longitudinal axis, (ii) the
142 vertical transfer toward the external atmosphere and (iii) the transport at street
143 intersections.

144 We introduce here two further simplifications to this approach. The first
145 concerns the model for the pollutant transfer at street intersections, which is

significantly different from that adopted by Soulhac et al. (2011). Secondly, we will neglect the dispersion occurring above roof level. Since our focus is on ground level releases only (therefore inducing maximal concentration at the street level, within the canopy), we will assume that the amount of pollutant transferred out of the streets, towards the overlying boundary layer, will not further contribute to the pollutant concentration in the downwind streets. In other words, we consider that this vertical flux of pollutants, from the canopy to the external atmosphere, will induce negligible concentrations above roof level (due to the high dilution occurring in the lower part of the boundary layer, compared to that within the streets) and that eventual mass flows from the overlying atmosphere towards the street canyons will not contribute significantly to ground level pollution. These two assumptions allow us to adapt the street network approach to the propagation model presented in Section 3 based on the formalism of the theory of complex networks.

In the following, the transport mechanisms along a street canyon and at street intersections are described in details. The emission scenario consists of a ground level and punctual release (s in Fig. 1) within the urban canopy. The external wind blowing on the city with direction Φ is the driving force for propagation processes.

2.1. Transport along a street canyon

Consider a source s releasing a gaseous substance that results in a concentration c_0 at the beginning of a street canyon, as illustrated in Fig. 1.b-c. The substance propagates horizontally due to the advective flux along the longitudinal axis, and vertically due to the turbulent flux between the street and the overlying atmosphere (Soulhac et al., 2013). A simple but exhaustive way to model these two mechanisms is the use of the one-dimensional transport equation

$$\frac{\partial c}{\partial t} + u_{st} \frac{\partial c}{\partial x} + \frac{u_d}{h} (c - c_{ext}) = 0, \quad (1)$$

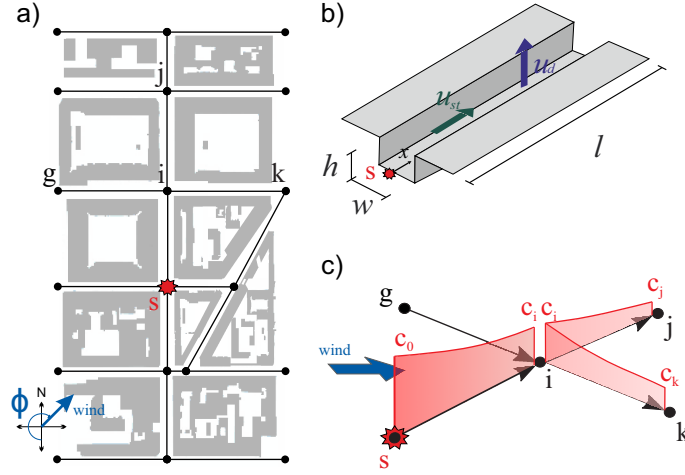


Figure 1: a) Toxic source s within a network of streets. Propagation is driven by the wind blowing on the city with direction Φ . b) Representation of a street canyon with the main variables of the model. c) Transport of a contaminated flow in street intersections.

173 whose solution is the function $c(x, t)$, i.e. the concentration along the longitudinal
 174 coordinate x over time t .

175 The first two terms in (1) describe the convective transport driven by the
 176 spatially averaged wind velocity along x (u_{st}). This velocity is assumed to
 177 be given by a balance between the stress imposed at the canopy top by the
 178 external atmospheric flow and the drag due to the roughness of the canyon walls
 179 (neglecting the role of pressure gradients). Under this assumption, Soulhac
 180 et al. (2008) derived an analytical formulation for u_{st} , as a function of the
 181 external wind intensity and direction, the geometry of the street canyon and the
 182 aerodynamic roughness of building walls (see Appendix A). The third term in (1)
 183 models the mass transfer from/to the canyon to/from the overlying atmosphere
 184 by means of a bulk exchange velocity u_d (Salizzoni et al., 2009) estimated as

$$u_d = \frac{u_*}{\sqrt{2\pi}}, \quad (2)$$

185 where u_* is the friction velocity of the overlying boundary layer flow. Assuming
 186 that pollutant concentration above the canopy, c_{ext} , is negligible compared to
 187 the concentration in the canyon, the vertical flux is unidirectional. This vertical

188 loss is the only decay term in the model, since it is assumed that the involved
 189 toxic substances do not undergo chemical or biological transformations or, in
 190 any case, have a reaction time longer than the time needed for propagation.

191 In (1), turbulent longitudinal diffusion is not considered as it is negligible
 192 with respect to the longitudinal advection.

193 Equation (1) was solved for both an instantaneous and a continuous release
 194 in the source (see Appendix B). In the first case, the initial condition is set
 195 as a rectangular pulse with height c_0 . The solution describes this initial step
 196 travelling along the street with velocity u_{st} and undergoing an exponential decay
 197 of concentration. In the second case, the initial condition is a continuous release
 198 with constant concentration c_0 . The solution is a front that spreads along the
 199 street with velocity u_{st} . Although the analytical solutions are different, the
 200 concentration at the end of the street ($x = l$) in both cases is the same:

$$c_l \left(x = l, t = \frac{l}{u_{st}} \right) = c_0 e^{-\frac{l}{u_{st}} \frac{u_d}{h}}. \quad (3)$$

201 Thus, the concentration at the beginning of the street (c_0) undergoes an expo-
 202 nential decay driven by the ratio between the advection time (l/u_{st}) that the
 203 toxic front spends to reach the end of the street, and the vertical transfer time
 204 (h/u_d). The terms in the exponent summarize all the information about the
 205 geometry of the canyon and the flow dynamics in it.

206 *2.2. Transport in the street intersections*

207 The flow field in the street intersections is driven by complex physical pro-
 208 cesses that depend on multiple geometric and meteorological parameters. Sev-
 209 eral studies (e.g. Hunter et al., 1990; Robins et al., 2002; Soulhac et al., 2009)
 210 have demonstrated that even slight variations in the building geometry and wind
 211 direction can affect significantly the redistribution of the incoming fluxes over
 212 the outgoing fluxes. On the basis of these observations, Soulhac et al. (2009)
 213 have developed a model, quantifying the balance of the time-averaged incoming
 214 and outgoing fluxes at the street intersection, depending on its geometry and

on the direction of the external wind. In defining the exchange model in the intersection for the pollutant propagation within the network we however adopt a different approach. Our aim is twofold: i) adopt a model which is the simplest as possible, and ii) adopt a conservative approach. With these aims we will consider that the concentration of pollutants at the beginning of the streets exiting the intersection is the one at the end of the incoming contaminated canyon.

Consider a simple intersection with a single incoming and one outgoing street canyon. The air flow entering the intersection with a concentration c_{in} is Q_{in} , while the air flow outgoing the intersection with a concentration c_{out} is Q_{out} . Two cases are possible for the mass balance in the intersection. In the first case, the mass flow from the incoming canyon ($\dot{m}_{in} = c_{in}Q_{in}$) is lower than the mass flow toward the outgoing canyon ($\dot{m}_{out} = c_{out}Q_{out}$). In order for the mass balance to be satisfied, an external mass flow (\dot{m}_{ext}) from the atmosphere above the canopy enters the intersection vertically with an air flow rate Q_{ext} and a concentration c_{ext} . Since it is assumed that the external concentration c_{ext} is negligible, this mass flow makes a zero contribution in the mass balance and c_{out} is given by $c_{out} = c_{in}Q_{in}/Q_{out}$. As the flow rate balance in the intersection is $Q_{in} + Q_{ext} = Q_{out}$, the ratio Q_{in}/Q_{out} is lower than 1 and thus $c_{out} < c_{in}$. In the second case, $\dot{m}_{in} > \dot{m}_{out}$ and the flow \dot{m}_{ext} leaves the intersection vertically. We consider that the concentration leaving the intersection is the same for both the upwards flow and the flow towards the outgoing street canyon, i.e. $c_{ext} = c_{out}$. Applying the mass ($c_{in}Q_{in} = c_{out}Q_{out} + c_{ext}Q_{ext}$) and flow rate ($Q_{in} = Q_{out} + Q_{ext}$) balance equations, we find that $c_{out} = c_{in}$. These arguments therefore show that our approach is conservative, i.e. tends to maximise the pollutant concentration in the downwind streets.

Similarly, in case of several streets crossing, we will affect the same concentration at the upwind section of all streets placed downwind the intersection. In other words, we are assuming that the pollutant puff reaching the intersection from a generic street will have a same probability of entering in any of the streets placed downwind the intersection. In doing so, we will consider the trajectories of all possible paths of the pollutant puffs that travel downwind their emission

246 point.

247 The assumptions adopted for the transport in street intersections are clearly
248 illustrated in Fig.1c. The contaminated flow from street (s, i) propagates to-
249 wards streets (i, j) and (i, k) . The street (g, i) is unspoiled, as it is shielded from
250 the wind that blows through the source of pollution. According to this scheme,
251 the concentration at the beginning of streets (i, j) and (i, k) is the one at the
252 end of street (s, i) .

253 3. A network perspective

254 In the model presented above, toxic substances move in the urban environ-
255 ment driven by the wind blowing along the street canyons. The street canyons
256 behave like upward leaking transport channels and their geometry, position and
257 connectivity strongly influence the propagation. In big cities, streets cross each
258 other to compose intricate patterns (Fig. 2). Given the spatial extent and the
259 high number of elements, these urban fabrics can be seen as complex networks
260 (Porta et al., 2006; Barthélemy, 2011). Links stand for the street canyons,
261 while nodes represent the street intersections. The direction and the weight
262 of the links describe the geometric and fluid-dynamics properties of the street
263 canyons. Within this approach, the tools of network theory provide interesting
264 information about the propagation phenomena.

265 3.1. Construction of the network

266 The urban canopy is modelled as a network of N nodes (intersections) and
267 M links (streets). Fictitious nodes can be created to divide a street into two
268 links in case there is a significant change in the street properties. Each link is
269 directed according to the orientation of the mean wind along the street (u_{st}).
270 Thus, the network structure represents both the topological properties of the
271 urban fabric and the directions in which the propagation processes take place.
272 The connectivity of the street canyons is described by the adjacency matrix \mathbf{A} ,
273 a $N \times N$ square matrix whose element A_{ij} is equal to 1 if a directed link from

node i to node j exists, is equal to 0 otherwise (see Appendix C for an example of adjacency matrix). Since the links have a specific direction, the adjacency matrix is asymmetric.

According to this network representation, the geometry and fluid-dynamics properties of the street canyons are stored efficiently in matrices. \mathbf{L} and \mathbf{H} are the symmetrical matrices of the length of the streets (l) and the average height of the buildings overlooking the streets (h). The wind velocity along the streets (u_{st}) and the velocity of the vertical transfer towards the external atmosphere (u_d) are enclosed in the matrices \mathbf{U} and \mathbf{U}_d .

As mentioned in the Introduction, the main purpose of this work is to establish a methodology for the rapid assessment of urban vulnerability to the ground-level release of toxic gases. The vulnerability index (V_s) for a generic node s can be defined as the number of people affected by the toxic propagation if the release takes place in s . The adopted network approach and matrix notation make it easy to calculate V_s as follows,

$$V_s = \sum_i^N \sum_j^N D_{ij} P_{ij}, \quad (4)$$

where \mathbf{P} is the matrix that associates at each link (i, j) the number of inhabitants per unit street length and \mathbf{D} is the matrix that associates at each link (i, j) the contaminated length of the street. This last matrix represents the zone of influence of the source node. The meaning of this matrix and its construction process will be widely described in Subsections 3.2 and 3.3.

An interesting advantage of this compact notation is that changes to the network properties can be easily implemented. By modifying matrices \mathbf{U} and \mathbf{U}_d , we can simulate different meteorological scenarios, while variations in population distribution (e.g., differences between weekdays and holidays) can be considered by adjusting \mathbf{P} . Furthermore, new buildings and structural changes are included in the model by revising the single elements of \mathbf{L} and \mathbf{H} .

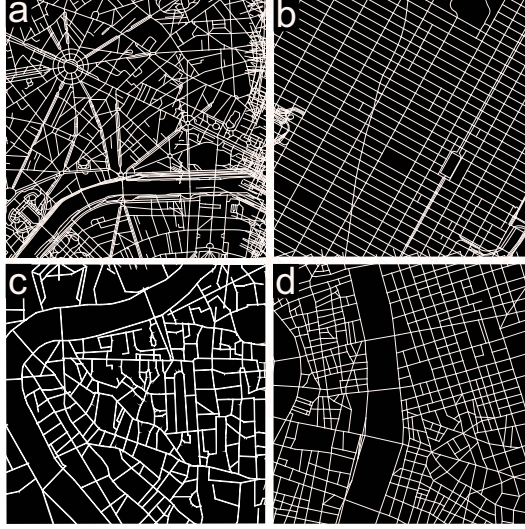


Figure 2: Snapshot of the street network of Paris (a), New York (b), Rome (c), and Lyon (d).

3.2. Propagation of a toxic substance in the street network

Consider the release of a toxic substance in a street intersection (see Fig. 3.a). According to the hypothesis of our model (Section 2), (i) the substance propagates along the adjacent streets depending on the direction of the wind, (ii) the concentration decays exponentially along the streets, (iii) the concentration at the end of each street can be estimated using (3), (iv) the concentration remains unchanged in the street intersections, and (v) from a contaminated street intersection the gas spreads further to the adjacent streets.

Given this description, the pollutant dispersion within the canopy can be then easily seen as a spreading process on a network (e.g., Newman, 2002; Comin and da Fontoura Costa, 2011). In Fig. 3.b the urban canopy is represented as a network. The links are directed according to the direction of the wind in the streets and the release is modelled as a source node s . From a network perspective, transport from s towards a generic node u is possible if there is a link directed from s to u , i.e. if (i) the two nodes are physically connected by a street canyon, and (ii) the wind is blowing from the source towards the target node. Once infected, the target node u is modelled as a new source

317 and the spreading process carries on towards the farthest nodes. According to
 318 this scheme, propagation is a recursive process that spontaneously expands to
 319 the topological boundaries of the network. Physically, the extent of the con-
 320 taminated zone can be delimited based on a threshold concentration value c_{th} :
 321 when the concentration falls below c_{th} , the contamination process is irrelevant.
 322 Thus, a stopping rule for the spreading process on the network is introduced:
 323 at each propagation hop the concentration at the target node is estimated. If
 324 this concentration is higher than c_{th} , then the propagation carries on.

325 Considering the example in Fig. 3.b, a toxic substance is released in the
 326 source node $s = 15$ and propagates towards the first neighbours of s : nodes 10,
 327 11, and 16. The concentration in the first neighbours is evaluated using Equation
 328 (3), as a function of the geometric and wind characteristics of the street canyons
 329 associated to links (15, 10), (15, 11) and (15, 16). Since the concentration in the
 330 first neighbours is greater than the predefined threshold c_{th} , nodes 10, 11 and
 331 16 act as source nodes and the spreading process carries on towards the second
 332 neighbours of s . In the same way, the third and fourth neighbours are affected
 333 by the toxic propagation until the concentration in the nodes falls below c_{th} .

334 According to this network interpretation, the spreading of a toxic gas in
 335 the urban environment is governed by two properties of the network: (i) the
 336 topological connectivity of the network, given by its adjacency matrix \mathbf{A} , and
 337 (ii) the concentration decay along the links, given by a combination of the
 338 geometric characteristics and the flow dynamics in the street canyons.

339 This spreading results in the zone of influence of the source node s , i.e.
 340 the set of links contaminated from the propagation process originated in s (the
 341 elements highlighted in blue in Fig. 3). The number of people that lives in
 342 the zone of influence represents the vulnerability index of s (V_s). Notice that
 343 this index contains both information on population density and meteorological
 344 conditions in the city. In fact, as will be shown in the following sections, its
 345 value changes drastically with the wind direction.

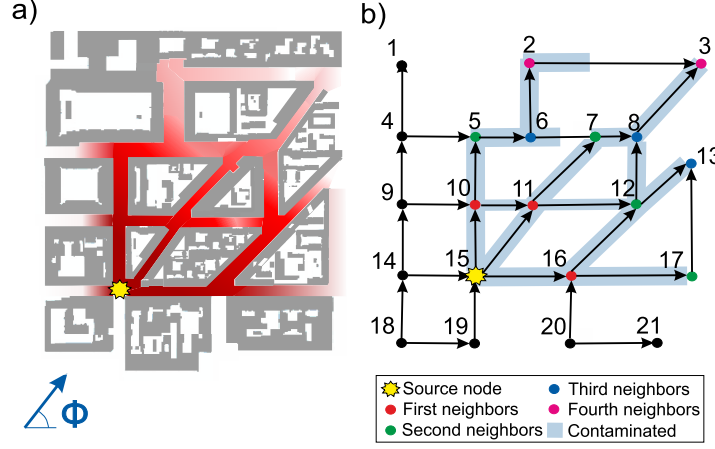


Figure 3: Analogy between the physical propagation of a toxic substance in the urban environment (a) and the spreading process on a network (b). Φ is the direction of the external wind blowing on the city.

3.3. Algorithm

Given a source node s with a concentration c_s , the set of its first neighbours $N_1(s)$ can be derived from the non-zero elements of the s -th row of the adjacency matrix \mathbf{A} . In Fig. 3, $s = 15$ and thus $N_1(s) = \{10, 11, 16\}$. For each node u belonging to the set $N_1(s)$, the algorithm calculates the distance D_{su}^{pot} . This length is the potential distance (hence the superscript *pot*) that the contaminated front can reach along the link (s, u) with a concentration higher than the predefined threshold c_{th} . According to (3), D_{su}^{pot} is

$$D_{su}^{pot} = -\frac{H_{su}}{U_{d,su}} U_{su} \log \left(\frac{c_{th}}{c_s} \right), \quad \forall u \in N_1(s). \quad (5)$$

In general, D_{su}^{pot} is different from the physical length of the street (L_{su}) associated to the link (s, u) . D_{su}^{pot} is lower than L_{su} if the concentration undergoes the threshold c_{th} before the propagation front has travelled the entire street. *Vice versa*, it is higher if the front reaches node u with a concentration above the threshold. As a consequence, the effective contaminated distance (D_{su}) is the minimum between the reachable distance D_{su}^{pot} and the effective length of

360 the street, i.e.

$$D_{su} = \min[D_{su}^{pot}, L_{su}] \quad (6)$$

361 If $D_{su} = L_{su}$, the substance has reached the target node u with a concen-
 362 tration equal to or higher than c_{th} . As a result, node u is contaminated. Con-
 363 versely, if the front reaches u with a negligible concentration (i.e. $D_{su} < L_{su}$),
 364 then node u remains unspoiled. In both cases, the algorithm stores the effective
 365 contaminated length D_{su} as the (s, u) element in the matrix \mathbf{D} . As introduced
 366 in Section 3.1, this matrix defines the zone of influence of the source node s .

367 We define $\hat{N}_1(s)$ the set of the first neighbours of s that have been contam-
 368 inated,

$$\hat{N}_1(s) = \{u \in N_1(s) \mid D_{su} = L_{su}\}. \quad (7)$$

369 Referring to Fig. 3, $\hat{N}_1(15) = \{10, 11, 16\}$ since all the first neighbours of
 370 s are contaminated. The algorithm estimates the concentration in the nodes
 371 belonging to $\hat{N}_1(s)$ using (3), as

$$c_u = c_s e^{-\frac{U_{d,su}}{H_{su}} \frac{L_{su}}{U_{su}}}, \quad \forall u \in \hat{N}_1(s). \quad (8)$$

372 These nodes behave as new source nodes. Thus, the algorithm repeats the above
 373 presented steps, replacing in Equations (5)-(8) node s with the nodes belonging
 374 to $\hat{N}_1(s)$. For example, once node 16 (Fig. 3) has been contaminated from
 375 the initial source node 15, the algorithm finds the set of its first neighbours,
 376 i.e. $N_1(16) = \{12, 17\}$. Equations (5)-(6) estimate the effective contaminated
 377 length along links (16, 12) and (16, 17), while (7) identifies the set of the first
 378 neighbours of node 16 that have been infected, i.e. $\hat{N}_1(16) = \{12, 17\}$. Finally,
 379 the concentration reached in nodes 12 and 17 is determined by (8). This proce-
 380 dure is repeated recursively until the concentration in each node of the network
 381 falls below the threshold c_{th} .

382 Notice that for nodes 15 and 16 the sets N_1 and \hat{N}_1 are identical. However,

383 this is not true in general. Consider node 6 in Fig. 3b. The set of its first neigh-
384 bours is $N_1(6) = \{2, 7\}$, while $\hat{N}_1(6) = \{2\}$ because node 7 cannot be reached
385 by the propagation along link (6, 7).

386

387 The algorithm explores the nodes of the network starting from a root node
388 and progressively visiting the adjacent nodes. In computer science, this process
389 is called tree traversal (Valiente, 2013) since the result of the exploration is a
390 tree structure that is a subgraph of the initial graph. In our study, this tree
391 corresponds to the zone of influence of the source node. There are multiple
392 ways to perform a tree traversal, according to the order in which the nodes are
393 visited. The algorithm presented above explores the nodes of the network using
394 a depth-first search analysis. The algorithm starts at the source node and goes
395 as far as it can down a given branch before backtracking. Referring to Fig.
396 3, the algorithm starts at node 15, selects the first node 10 in the set $\hat{N}_1(15)$
397 and deepens the analysis in the first element of the set $\hat{N}_1(10)$, i.e. node 5.
398 Following this ratio, the algorithm visits the nodes in the order (15, 10, 5, 6, 2).
399 The in-depth analysis along this path ends when the concentration falls below
400 the threshold c_{th} . Formally, the path (15, 10, 5, 6, 2) ends because the set $\hat{N}_1(2)$
401 is empty. Once the first branch has been explored, the algorithm backtracks to
402 node 6's next available neighbour, i.e. node 7.

403 From the numerical point of view, depth-first search analysis requires less
404 memory and it is more efficient in finding trees on networks compared to other
405 algorithms, such as breath-first search (Kozen, 1992).

406 Notice that, referring to the example in Fig. 3b, link (11, 7) is affected
407 by toxic propagation twice, both along propagation path $\gamma_1=(15, 11, 7)$ and
408 $\gamma_2=(15, 10, 11, 7)$. As a consequence the algorithm calculates two different
409 values of $D_{11,7}$, since the concentration reached at node 11 (c_{11}) along γ_1 is
410 generally different from the one obtained along γ_2 . As the aim of the elaboration
411 is to determine the extent of the zone of influence, the algorithm considers all the
412 possible passages through a generic link and stores the longest distance reached
413 by the toxic substance. In details, for each path γ_α the algorithm compares

414 $D_{su}^{(\gamma_\alpha)}$ with the distance $D_{su}^{(\gamma_{\alpha-1})}$ obtained along the previously explored path
 415 $\gamma_{\alpha-1}$ passing through the link (s, u) . Equation (6) is, thus, refined as:

$$D_{su}^{(\gamma_\alpha)} = \max[\min[D_{su}^{pot}, L_{su}], D_{su}^{(\gamma_{\alpha-1})}], \quad (9)$$

416 where γ_α is an index for the order in which the path is explored.

417 4. Results

418 The potentials of the proposed approach are discussed through a case study.
 419 The model is applied to assess urban vulnerability of the city of Lyon (France)
 420 to the release of a toxic gas. Lyon (Fig. 4) is located in east-central France and
 421 it is the third-largest urban agglomeration in France after Paris and Marseille,
 422 with a population of approximately 1.5 million inhabitants. In this work, the
 423 analysis is limited to a part of the city (Fig. 4c) that presents an intricate urban
 424 fabric and tall buildings on the edge of the streets. These characteristics are
 425 consistent with the model representation of the streets as a network of street
 426 canyons. The study area has an extent of about 6.5 km^2 , it hosts a population of
 427 about 140,000 inhabitants and is delimited by natural and artificial boundaries
 428 (rivers, parks and railways). These boundaries determine a discontinuity in the
 429 dispersion of pollutants along the street canyons.

430 The street canyons and the street intersections result in a network of 750
 431 nodes and 1110 links. The geometric characteristics of the street canyons, the
 432 population density, the longitudinal mean wind and the vertical transfer velocity
 433 in the streets are stored in the matrices \mathbf{H} , \mathbf{L} , \mathbf{P} , \mathbf{U} and \mathbf{U}_d , respectively.

434 4.1. The zone of influence of a source node

435 The first outcome of the elaboration is the identification of the zone of influ-
 436 ence of a source node, i.e. the set of links contaminated by the toxic substance
 437 with a concentration above a defined threshold, stored in matrix \mathbf{D} (see Section
 438 3).

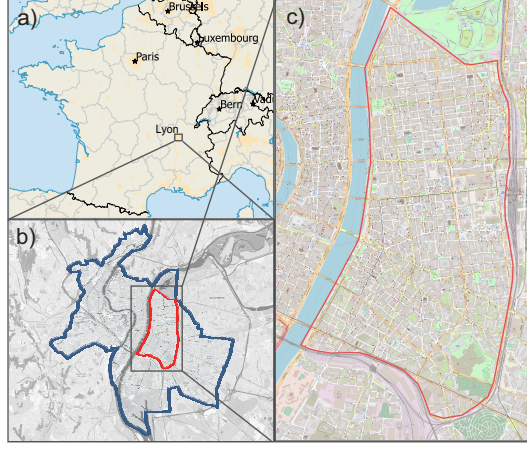


Figure 4: The case study area. a) Location of the metropolitan area of Lyon within France. b) Location of the study area within the municipality of Lyon. c) The study area.

As an example, Fig. 5 shows the zone of influence of a source node for different wind directions ($\Phi = 45^\circ, 135^\circ, 225^\circ$ and 315°) and for two different initial concentration values. For the sake of generality, the concentration scenarios are defined by the ratio between the concentration in the source node (c_0) and the limit concentration (c_{th}).

The urban topology, the wind direction and the initial concentration shape the zone of influence of the source node. Variations in the mean velocity of the external wind (\bar{u}) as well as the stability conditions (as determined by the Monin-Obukhov length L_{MO}) are instead irrelevant. As stated in (2) and (A.1)-(A.2), both u_d and u_{st} linearly depend on the friction velocity u_* . Since our propagation model evaluates the pollutant spreading as a function of their ratio (3), variations of u_* , and thus of L_{MO} and \bar{u} , will not be effective in determining the zone of influence.

4.2. Spatial and frequency distribution of urban vulnerability

The spatial pattern of urban vulnerability can be analysed at a glance using vulnerability maps. Given the geometry of the urban fabric, the conditions of the external wind, the spatial distribution of the citizens and the emission scenario, the model provides in a short time (from a few seconds to a few minutes

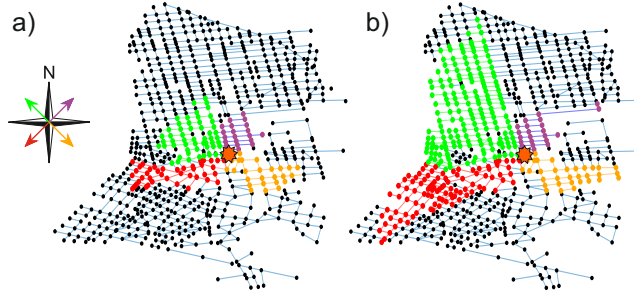


Figure 5: The zone of influence of a generic source node (orange star) in the network for different wind directions (red, green, violet and yellow refer to the wind directions $\Phi = 45^\circ$, 135° , 225° and 315° , respectively). Panel (a) and (b) refer to a concentration ratio $c_0/c_{th} = 10$ and $c_0/c_{th} = 100$, respectively.

457 depending on the concentration ratio c_0/c_{th}) a map that associates at each node
 458 of the street network its vulnerability index. To do this, the algorithm for the
 459 spread of toxic substances on networks (Section 3) is applied and the matrix of
 460 the contaminated street lengths \mathbf{D} (i.e. the zone of influence) is computed for all
 461 nodes of the network. Next, the vulnerability index defined in Equation (4) is
 462 calculated for each node, taking into account both the extent of the zone affected
 463 by the propagation originated in the node (\mathbf{D}) and the number of people leaving
 464 in that zone (\mathbf{P}). Finally, a vulnerability map is constructed by associating a
 465 colour to each node based on its vulnerability index.

466 Sixteen vulnerability maps for the case study area are obtained (see the
 467 supplementary material) by varying the direction of the external wind (Φ) and
 468 the concentration ratio c_0/c_{th} . These parameters affect the node vulnerability
 469 by shaping its zone of influence (matrix \mathbf{D}), as mentioned in Section 4.1. In
 470 this study, the number of inhabitants in the streets (\mathbf{P}) was kept constant in
 471 the different scenarios and was derived from the map of the resident citizens in
 472 the city of Lyon. Future works should consider how the spatial distribution of
 473 the population varies on different days of the week or at different times of the
 474 day. These variations could be easily implemented in the model by modifying
 475 the \mathbf{P} matrix and would increase the number of cases (i.e. maps) considered.

476 Fig. 6 shows four vulnerability maps for a wind direction varying between
 477 $\Phi = 0^\circ$ (north wind) and $\Phi = 135^\circ$. The maps are obtained simulating for

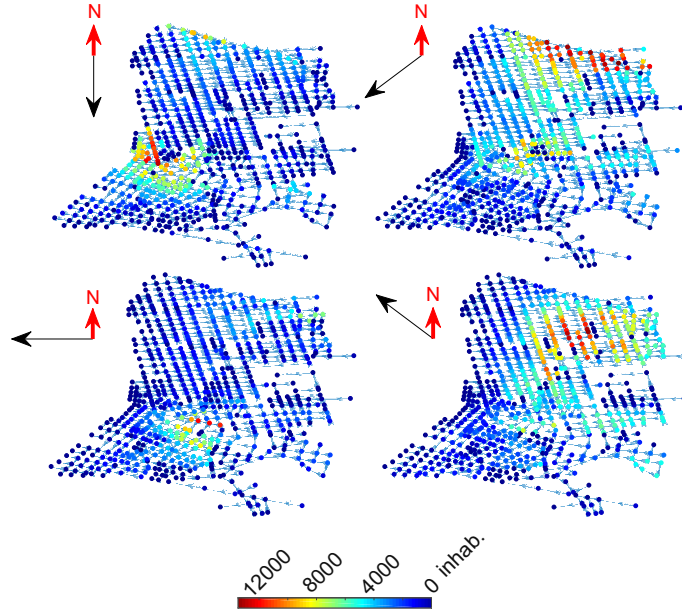


Figure 6: Vulnerability maps for different wind directions and with a concentration ratio c_0/c_{th} equal to 10.

each node a release with a concentration equal to ten times the threshold value,
i.e. $c_0/c_{th} = 10$. Node vulnerability, defined in terms of affected people, varies
between 0 (blue) and 12000 (red) inhabitants. The maps reveal at a glance
the most susceptible areas and the global vulnerability of the urban fabric in
the different wind direction scenarios. From Fig. 6, it can be seen that the
vulnerability index is not distributed homogeneously. On the contrary, the
vulnerability tends to be maximal (red nodes) in a defined area of the map and
its value gradually decreases in the nodes around it. Moreover, the position
of the most vulnerable nodes varies strongly with small variations in the wind
direction. As an example, notice the difference between the two scenarios related
to $\Phi = 0^\circ$ and $\Phi = 45^\circ$ in Fig. 6.

To better understand this behaviour, Fig. 7.a summaries the results of the
sixteen simulated scenarios. Each scenario is represented by an arrow oriented
with the wind direction, coloured according to the concentration ratio and po-
sitioned in the area of greatest vulnerability for that scenario. It is evident that

493 for Φ equal to 0° , 90° , 180° and 270° (the cardinal directions) the most vulner-
 494 able nodes are located in the southern part of the network, while for Φ equal to
 495 45° , 135° , 225° and 315° (the transversal directions) the most vulnerable areas
 496 are in the northern part of the network.

497 As the geometric characteristics of the street canyons and the population
 498 density are rather homogeneously distributed in the street network, this differ-
 499 ent vulnerability pattern is related to the orientation of the streets with respect
 500 to the wind direction. The northern part of the street network is mainly ori-
 501 ented according to the cardinal directions (North-South and West-East oriented
 502 streets). As the wind blows in one of these directions (e.g., $\Phi = 0^\circ$), only the
 503 aligned streets (i.e. the North-South oriented streets) are affected by the prop-
 504 agation of toxic substances, while the orthogonal streets (i.e. the East-West
 505 oriented streets) are completely shielded from the wind. This condition limits
 506 the extent of the zone of influence of a generic source node. Conversely, as the
 507 wind blows according to one of the transversal direction, the propagation affects
 508 both the North-South and the East-West oriented streets, thus increasing the
 509 vulnerability. As the southern part of the street network is oriented mainly
 510 according to the transverse directions, a greater vulnerability will occur when
 511 the wind is blowing in the cardinal directions.

512 For each of the sixteen scenarios analysed, the average vulnerability over the
 513 entire network (\bar{V}) is calculated as

$$\bar{V} = \frac{1}{N} \sum_i^N V_i, \quad (10)$$

514 where V_i is the vulnerability index for the i -th node and N is the number of
 515 nodes in the network. The two polar histograms of Fig. 7.b report these average
 516 vulnerability values for the two concentration ratios considered. Each sector in
 517 the polar histograms refers to a different wind direction. As expected, higher
 518 concentration ratios correspond to higher vulnerability values. Moreover, since
 519 most of the streets ($\sim 60\%$) are oriented in the cardinal directions, the average
 520 vulnerability is greater when the wind blows in the transversal directions.

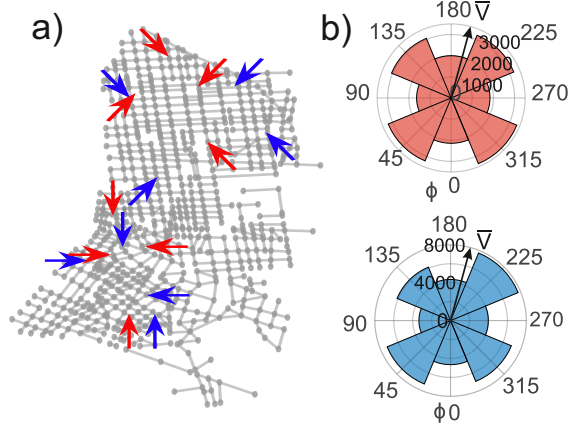


Figure 7: a) Most vulnerable areas in the street network for different wind directions and concentration ratios. Each scenario is represented by an arrow oriented according to the wind direction, coloured according to the concentration ratio (red arrows for $c_0/c_{th} = 10$ and blue arrows for $c_0/c_{th} = 100$) and positioned in the area of greatest vulnerability on the map. b) Polar histogram (red for $c_0/c_{th} = 10$ and blue for $c_0/c_{th} = 100$) of the average node vulnerability for the different wind directions

Fig. 8 gives an overview of the long-term vulnerability of the urban fabric to toxic releases. The maps depict nodes vulnerability weighted by the annual frequency of the wind directions over the city of Lyon. As detailed in the inset of Fig. 8, the dominant wind direction in Lyon is North-South. As a consequence, the highest vulnerabilities are located in the circled area, corresponding to the regions mostly stressed by North-South oriented winds (see $\Phi = 0^\circ$ and $\Phi = 180^\circ$ scenarios in the supplementary material).

Results in Fig. 6 suggest that, for each scenario, a restricted area of the urban fabric is characterized by high levels of vulnerability, while most of the streets are not exposed. Thus, both spatial and frequency distribution of node vulnerabilities are not trivial. A frequency analysis of vulnerability values was performed to identify an eventual significant statistical distribution of the data. For each scenario, node vulnerability values were classified in ten equal size intervals. Then, the relative frequency (p) of each class was calculated. Fig. 9

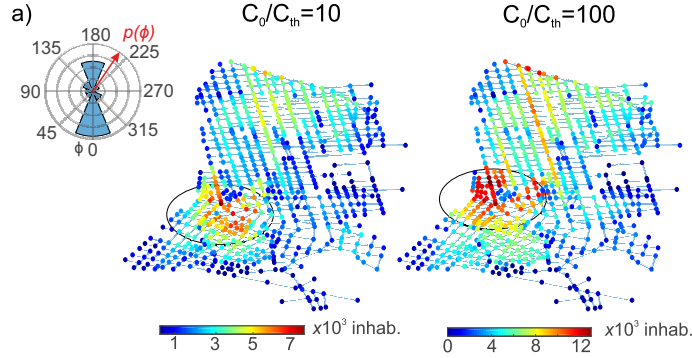


Figure 8: Maps of vulnerability weighted by the annual frequency of the wind directions. The polar histogram (inset *a*) shows the occurrence of wind directions in the city of Lyon in terms of annual relative frequency $p(\Phi)$.

535 presents the relative frequency of node vulnerability for the different scenarios
 536 in a log-log plot. For the sake of graphic clarity, vulnerability values were
 537 normalised to the maximum one (V_{max}). Generally, the data show a linear
 538 behaviour in the log-log plot, thus exhibiting a power law trend. The power law
 539 confirms that vulnerability distribution is heterogeneous, with few nodes being
 540 much more critical than the others. This hierarchical configuration suggests
 541 that, for each wind scenario, the entire neighbourhood could be protected with
 542 security interventions targeted on small urban areas.

543 Notice that many real-world networks (e.g., the Internet, World Wide Web,
 544 scientific citations) present a power law distribution of nodes degree (Boccaletti
 545 et al., 2006). The degree defines the importance of a node in the network
 546 in terms of its connectivity. In this case, a power law results from the not
 547 trivial interaction of multiple factors that define the vulnerability index, i.e.
 548 the topological connectivity of the network, the geometry characteristics of the
 549 street canyons, the toxic spreading process and the population distribution in
 550 the city.

551 5. Conclusions

552 We have presented an innovative approach for the study of diffusion pro-
 553 cesses in the urban atmosphere. Within the urban canopy, the wind flows along

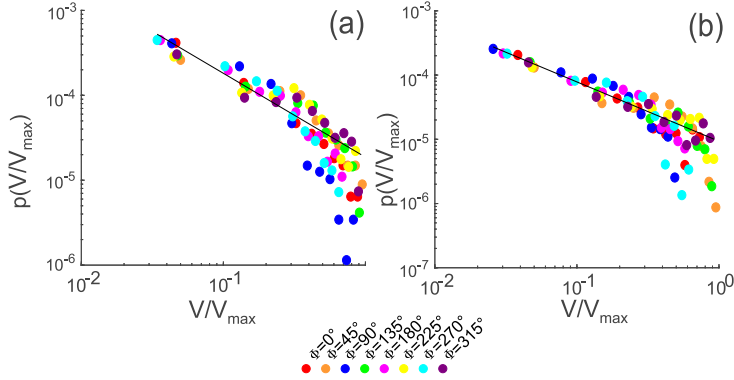


Figure 9: Relative frequency of vulnerability for different wind directions and for a concentration ratio $c_0/c_{th} = 10$ (a) and $c_0/c_{th} = 100$ (b). The display is in logarithmic scale.

the street canyons and the transport of pollutants is strongly influenced by the structure of the city, i.e. by the orientation of the streets and by their interconnections. Moving from these considerations, we have modelled the interaction between the city and the external wind as a weighted complex network whose links and nodes represent the streets and the street intersections, respectively. The direction of the links and their weights describe the direction and the intensity of the wind along the streets and the geometric properties of the buildings that surround the street canyons. Using a depth-first search analysis, we have implemented a spreading model on networks that simulates the propagation process from a point source. As an example, the developed method has been adopted to create vulnerability maps of the city of Lyon (France). These maps highlight the most vulnerable areas of the city, i.e. the areas from which the spread of a toxic substance, released at ground level, can damage more people. We found that the spatial and frequency distribution of urban vulnerability is heterogeneous and is strongly influenced by the alignment between the direction of the external wind and the orientation of the streets.

The model proved to be quick and functional and therefore useful for the analysis of multiple scenarios that take into account various meteorological conditions or different distributions of the residing population. Thanks to these characteristics, this method is suitable for the prediction and management of

574 emergency scenarios, due to accidental or harmful releases of toxic substances
575 in the urban atmosphere.

576 This work is in line with recent efforts to develop operational modelling tools
577 for the prediction of pollutant transport in large urban areas. Moreover, the
578 study demonstrate that the innovative tools of the theory of complex networks
579 can be adopted to this aim. The frequency with which new techniques and
580 applications are developed in the field of complex networks makes this new
581 perspective particularly promising.

582 Future work is aimed at comparing different cities to understand how urban
583 topology influences the diffusive process and therefore the vulnerability of the
584 city. In this way, it will be possible to understand which cities are the most
585 structurally fragile. Further analyses should be conducted to consider variations
586 in urban vulnerability due to changes in the presence of people in the different
587 times of the day or during the different periods of the week. Finally, the results
588 encourage a deeper understanding of the link between the theory of complex
589 networks and the problems of diffusion in the urban environment.

590 **Appendix A. Longitudinal wind velocity along a street canyon**

591 According to Soulhac et al. (2008), the average velocity u_{st} along the longi-
592 tudinal axis of a street canyon reads

$$u_{st} = u_H \cos \Phi \frac{\delta_i^2}{hw} \left[\frac{2\sqrt{2}}{C} (1 - \beta) \left(1 - \frac{C^2}{3} + \frac{C^4}{45} \right) + \beta \frac{2\alpha - 3}{\alpha} + \left(\frac{w}{\delta_i} - 2 \right) \frac{\alpha - 1}{\alpha} \right] \quad (\text{A.1})$$

$$\text{with} = \begin{cases} \alpha = \ln \left(\frac{\delta_i}{z_{0,build}} \right) \\ \beta = \exp \left[\frac{C}{\sqrt{2}} \left(1 - \frac{h}{\delta_i} \right) \right] \\ u_H = u_* \sqrt{\frac{\pi}{\sqrt{2}k^2C} \left[Y_0(C) - \frac{J_0(C)Y_1(C)}{J_1(C)} \right]} \\ C \text{ solution of } \frac{z_{0,build}}{\delta_i} = \frac{2}{C} \exp \left[\frac{\pi}{2} \frac{Y_1(C)}{J_1(C)} - \gamma \right] \\ \delta_i = \min \left(h, \frac{w}{2} \right) \end{cases} \quad (\text{A.2})$$

where Φ is the external wind direction with respect to the street longitudinal axis, h and w are the height and the width of the street canyon, $z_{0,build}$ is the aerodynamic roughness of the canyon walls, u_* is the friction velocity of the external atmospheric boundary layer flow, J_0 , J_1 , Y_0 and Y_1 are Bessel functions, k is the von Kármán constant, and γ is the Euler constant. The friction velocity u_* is determined using the Monin-Obukhov similarity theory to model the flow in the external boundary layer.

Appendix B. Solution for the one-dimensional transport equation

Under the assumption that c_{ext} is negligible with respect to the concentration in the street canyon, the one-dimensional transport equation (1) becomes

$$\frac{\partial c}{\partial t} + u_{st} \frac{\partial c}{\partial x} + \frac{u_d}{h} c = 0. \quad (\text{B.1})$$

By introducing the substitution

$$g(x, t) = c(x, t) \exp \left(\frac{u_d}{h} t \right), \quad (\text{B.2})$$

(B.1) yields

$$\frac{\partial g}{\partial t} + u_{st} \frac{\partial g}{\partial x} = 0. \quad (\text{B.3})$$

The general solution for (B.3) is found by introducing the new coordinates $\tau = t$, $\xi = x - u_{st}t$ and using the chain rule:

$$\frac{\partial g(x, t)}{\partial t} = \frac{\partial g(\xi, \tau)}{\partial \tau} - u_{st} \frac{\partial g(\xi, \tau)}{\partial \xi} \quad (\text{B.4})$$

$$\frac{\partial g(x, t)}{\partial x} = \frac{\partial g(\xi, \tau)}{\partial \xi}. \quad (\text{B.5})$$

Equation (B.3) becomes

$$\frac{\partial g(\xi, \tau)}{\partial \tau} = 0, \quad (\text{B.6})$$

and, therefore,

$$g(\xi, \tau) = F(\xi) \quad \rightarrow \quad g(x, t) = F(x - u_{st}t), \quad (\text{B.7})$$

where F is a derivable function. The solution of (B.1) is obtained returning to the original function,

$$c(x, t) = g(x, t) \exp\left(-\frac{u_d}{h}t\right) = F(x - u_{st}t) \exp\left(-\frac{u_d}{h}t\right). \quad (\text{B.8})$$

Function F is found using the initial or boundary conditions of the problem.

For a continuous release c_0 in the source node starting from $t \geq 0$, the boundary condition is defined as

$$c(0, t) = c_0 \Theta(t), \quad (\text{B.9})$$

where Θ is the Heaviside function. For $x = 0$, (B.8) and (B.9) yield

$$c(0, t) = F(-u_{st}t) \exp\left(-\frac{u_d}{h}t\right) = c_0 \Theta(t). \quad (\text{B.10})$$

Function F is obtained from the previous one and the solution for the continuous release is thus

$$c(x, t) = F(x - u_{st}t) \exp\left(-\frac{u_d}{h}t\right) = c_0 \exp\left(-\frac{u_d}{u_{st}} \frac{x}{h}\right) \Theta\left(t - \frac{x}{u_{st}}\right). \quad (\text{B.11})$$

617 For a quick release in the source node, the initial condition is set as a rect-
618 angular pulse with width a and height c_0

$$c(x, 0) = c_0[\Theta(x) - \Theta(x - a)]. \quad (\text{B.12})$$

619 When a tends to zero, the release is almost instantaneous. Following the same
620 reasoning as in (B.10) and (B.11), but considering this time $t = 0$, we obtain
621 the solution for a quick release:

$$c(x, t) = c_0 \exp\left(-\frac{u_d}{h}t\right) [\Theta(x - u_{st}t) - \Theta(x - u_{st}t - a)]. \quad (\text{B.13})$$

622 Appendix C. Adjacency matrix

623 Consider the network in Fig.1c, extracted as a subgraph from the network
624 of streets in Fig.1a. The adjacency matrix of this simple four-links graph reads

$$\mathbf{A} = \begin{matrix} & \begin{matrix} s & g & i & j & k \end{matrix} \\ \begin{matrix} s \\ g \\ i \\ j \\ k \end{matrix} & \begin{pmatrix} 0 & 0 & 1 & 0 & 0 \\ 0 & 0 & 1 & 0 & 0 \\ 0 & 0 & 0 & 1 & 1 \\ 0 & 0 & 0 & 0 & 0 \\ 0 & 0 & 0 & 0 & 0 \end{pmatrix} \end{matrix}. \quad (\text{C.1})$$

625 Note that the matrix is asymmetric since the network is directed (i.e. the links
626 have a specific direction).

627 References

- 628 Ahern, J., 2011. From fail-safe to safe-to-fail: Sustainability and resilience in
629 the new urban world. *Landscape and Urban Planning* 100 (4), 341–343.
- 630 Arnfield, A. J., 2003. Two decades of urban climate research: A review of turbu-
631 lence, exchanges of energy and water, and the urban heat island. *International*
632 *Journal of Climatology* 23 (1), 1–26.

633 Barthélemy, M., 2011. Spatial networks. *Physics Reports* 499 (1-3), 1–101.

634 Berke, P. R., Song, Y., Stevens, M., 2009. Integrating hazard mitigation into
635 new urban and conventional developments. *Journal of Planning Education*
636 and Research 28 (4), 441–455.

637 Blocken, B., 2015. Computational Fluid Dynamics for urban physics: Importance, scales, possibilities, limitations and ten tips and tricks towards accurate
638 and reliable simulations. *Building and Environment* 91, 219–245.

640 Boccaletti, S., Latora, V., Moreno, Y., Chavez, M., Hwang, D.-U., 2006. Complex networks: Structure and dynamics. *Physics Reports* 424 (4-5), 175–308.

641
642 Borgatti, S. P., Mehra, A., Brass, D. J., Labianca, G., 2009. Network analysis
643 in the social sciences. *Science* 323 (5916), 892–895.

644 Brunekreef, B., Holgate, S. T., 2002. Air pollution and health. *The Lancet*
645 360 (9341), 1233–1242.

646 Carruthers, D., Edmunds, H., Lester, A., McHugh, C., Singles, R., 2000. Use
647 and validation of ADMS-Urban in contrasting urban and industrial locations.
648 *International Journal of Environment and Pollution* 14 (1-6), 364–374.

649 Carvalho, R., Buzna, L., Bono, F., Gutiérrez, E., Just, W., Arrowsmith, D.,
650 2009. Robustness of trans-European gas networks. *Physical Review E* 80 (1),
651 016106.

652 Comin, C. H., da Fontoura Costa, L., 2011. Identifying the starting point of a
653 spreading process in complex networks. *Physical Review E* 84 (5), 056105.

654 Di Sabatino, S., Buccolieri, R., Salizzoni, P., 2013. Recent advancements in
655 numerical modelling of flow and dispersion in urban areas: A short review.
656 *International Journal of Environment and Pollution* 7 52 (3-4), 172–191.

657 Gelbrecht, M., Boers, N., Kurths, J., 2017. A complex network representation of
658 wind flows. *Chaos: An Interdisciplinary Journal of Nonlinear Science* 27 (3),
659 035808.

660 Giustolisi, O., Ridolfi, L., 2014. A novel infrastructure modularity index for
661 the segmentation of water distribution networks. *Water Resources Research*
662 50 (10), 7648–7661.

663 Heinrich, J., Wichmann, H.-E., 2004. Traffic related pollutants in Europe and
664 their effect on allergic disease. *Current Opinion in Allergy and Clinical Im-*
665 *munology* 4 (5), 341–348.

666 Hunter, L. J., Watson, I., Johnson, G., 1990. Modelling air flow regimes in urban
667 canyons. *Energy and Buildings* 15 (3-4), 315–324.

668 Kozen, D. C., 1992. Depth-first and breadth-first search. In: *The Design and*
669 *Analysis of Algorithms*. Springer, pp. 19–24.

670 Mayer, H., 1999. Air pollution in cities. *Atmospheric Environment* 33 (24-25),
671 4029–4037.

672 McLeish, C., 2017. Recasting the threat of chemical terrorism in the EU: The is-
673 sue of returnees from the syrian conflict. *European Journal of Risk Regulation*
674 8 (4), 643–657.

675 Namdeo, A., Colls, J., 1996. Development and evaluation of SBLINE, a suite of
676 models for the prediction of pollution concentrations from vehicles in urban
677 areas. *Science of the Total Environment* 189, 311–320.

678 Newman, M., 2010. *Networks: An introduction*. Oxford university press.

679 Newman, M. E., 2002. Spread of epidemic disease on networks. *Physical Review*
680 E 66 (1), 016128.

681 Oke, T. R., 1982. The energetic basis of the urban heat island. *Quarterly Journal*
682 *of the Royal Meteorological Society* 108 (455), 1–24.

683 Porta, S., Crucitti, P., Latora, V., 2006. The network analysis of urban streets:
684 A dual approach. *Physica A: Statistical Mechanics and its Applications*
685 369 (2), 853–866.

686 Robins, A., Savory, E., Scaperdas, A., Grigoriadis, D., 2002. Spatial variability
687 and source-receptor relations at a street intersection. *Water, Air and Soil*
688 *Pollution: Focus* 2 (5-6), 381–393.

689 Roth, M., 2000. Review of atmospheric turbulence over cities. *Quarterly Journal*
690 *of the Royal Meteorological Society* 126 (564), 941–990.

691 Salizzoni, P., Soulhac, L., Mejean, P., 2009. Street canyon ventilation and at-
692 mospheric turbulence. *Atmospheric Environment* 43 (32), 5056–5067.

693 Ser-Giacomi, E., Rossi, V., López, C., Hernandez-Garcia, E., 2015. Flow net-
694 works: A characterization of geophysical fluid transport. *Chaos: An Interdis-*
695 *ciplinary Journal of Nonlinear Science* 25 (3), 036404.

696 Soulhac, L., Garbero, V., Salizzoni, P., Mejean, P., Perkins, R., 2009. Flow and
697 dispersion in street intersections. *Atmospheric Environment* 43 (18), 2981–
698 2996.

699 Soulhac, L., Perkins, R. J., Salizzoni, P., 2008. Flow in a street canyon for any
700 external wind direction. *Boundary-Layer Meteorology* 126 (3), 365–388.

701 Soulhac, L., Salizzoni, P., Cierco, F.-X., Perkins, R., 2011. The model SIRANE
702 for atmospheric urban pollutant dispersion; part I, presentation of the model.
703 *Atmospheric Environment* 45 (39), 7379–7395.

704 Soulhac, L., Salizzoni, P., Mejean, P., Perkins, R., 2013. Parametric laws to
705 model urban pollutant dispersion with a street network approach. *Atmo-*
706 *spheric Environment* 67, 229–241.

707 Tominaga, Y., Stathopoulos, T., 2012. CFD modeling of pollution dispersion in
708 building array: Evaluation of turbulent scalar flux modeling in RANS model
709 using LES results. *Journal of Wind Engineering and Industrial Aerodynamics*
710 104, 484–491.

711 Tucker, J. B., 2000. *Toxic terror: Assessing terrorist use of chemical and bio-*
712 *logical weapons*. MIT Press.

- 713 Valiente, G., 2013. Algorithms on trees and graphs. Springer Science & Business
714 Media.
- 715 Yazdani, A., Jeffrey, P., 2011. Complex network analysis of water distribution
716 systems. Chaos: An Interdisciplinary Journal of Nonlinear Science 21 (1),
717 016111.

Supplementary Material

[Click here to download Supplementary Material: Supplementary_material.pdf](#)